RESEARCH ARTICLE

Society For Biomaterials

WILEY

Subsidence of a partially porous titanium lumbar cage produced by electron beam melting technology

Fabio Distefano[1] | Gabriella Epasto[1] | Eugenio Guglielmino[1] | Aurora Amata[2] | Rosalia Mineo[3]

[1]Department of Engineering, University of Messina, Messina, Italy

[2]ABR Srl, Zona Industriale Dittaino, Assoro, Italy

[3]Mt Ortho srl, via fossa lupo sn Aci Sant'Antonio, Catania, Italy

Correspondence
Gabriella Epasto, Department of Engineering, University of Messina, Contrada di Dio, Vill. Sant'Agata, 98166 Messina, Italy.
Email: gabriella.epasto@unime.it

Abstract

The lumbar intervertebral devices are widely used in the surgical treatment of lumbar diseases. The subsidence represents a serious clinical issue during the healing process, mainly when the interfaces between the implant and the vertebral bodies are not well designed. The aim of this study is the evaluation of subsidence risk for two different devices. The devices have the same shape, but one of them includes a filling micro lattice structure. The effect of the micro lattice structure on the subsidence behavior of the implant was evaluated by means of both experimental tests and finite element analyses. Compressive tests were carried out by using blocks made of grade 15 polyurethane, which simulate the vertebral bone. Non-linear, quasi-static finite element analyses were performed to simulate experimental and physiologic conditions. The experimental tests and the FE analyses showed that the subsidence risk is higher for the device without micro lattice structure, due to the smaller contact surface. Moreover, an overload in the central zone of the contact surface was detected in the same device and it could cause the implant failure. Thus, the micro lattice structure allows a homogenous pressure distribution at the implant–bone interface.

KEYWORDS
electron beam melting, finite element analysis, lumbar Interbody fusion, porous structures, TiAl-based alloy

1 | INTRODUCTION

The lumbar intervertebral body fusion devices are widely used in the treatment of lumbar diseases.[1] The subsidence of the implant[2,3] is one of the post-surgical complications of such devices during the healing process, and it can lead to the implant failure and to the collapse of the intervertebral body.[4,5] The risk factors associated with the subsidence of a titanium cage, such as age, sex, operation level, device geometry, alignment in the intervertebral bodies and global Hounsfield Units, were analyzed to facilitate an optimal management of such a condition.[6] The role of the intervertebral discs, which ensure

mechanical stability and prevent the implant subsidence, was investigated by determining their influence on the vertebral mechanical properties during axial compression tests[7] or by carrying out a finite element sensitivity study.[8] Many studies aim to predict the risk of subsidence for the intervertebral body fusion devices by means of finite element (FE) analysis[9] or statistical methods based on computed tomography (CT) scans.[10] FE analyses were carried out by applying different compressive intervertebral loads corresponding to some activities for investigating their influence on the generation of endplate stresses that increase the risk of subsidence.[11] Numerical analysis was also applied to assess the risk of subsidence by evaluating the

stresses at the interface between cage and vertebrae as functions of cage height and cage placement strategy: oblique asymmetric or anterior symmetric.[12] Other researchers calculated the contact area between implants and bone and evaluated the subsidence by modifying their angular mismatch,[13] or by calculating the rate of subsidence on upper and lower endplates of vertebral bodies using CT scans.[14] Several studies tried to improve the subsidence behavior of the implants by optimizing their designs. Shape optimization was performed by combining results of the experimental tests and CT scans, to identify the parts to be improved.[15] In another study, shape optimization was performed by means of FE analysis, developing a simulation based on genetic algorithm.[16]

Some studies applied the ASTM F2267 standard testing method to establish a range of mechanical properties that improve the subsidence behavior.[17] The correlation between cage size and subsidence was assessed by testing cages between two polyurethane foam blocks and the resistance achievable with larger cages was quantified. Yuan et al.[18] compared the subsidence resistance of transformational lumbar interbody fusion (TLIF) devices and lateral lumbar interbody fusion (LLIF) devices of different sizes under compression loading. In another study, Chong et al.[19] investigated three different sizes of lumbar devices under axial compression and rotation loads.

In this research paper, the risk of subsidence was analyzed for two different types of lumbar intervertebral body fusion devices. The first implant was characterized by the presence of both porous and solid structures; the second implant had only a solid structure (not filled), with the same shape of the first case. Moreover, the first case included a micro lattice core and micro lattice endplates at the interfaces between the implant and the intervertebral bodies. The contact pressure at the interface between implants and intervertebral bodies was calculated by means of experimental tests and FE models. Particular attention was paid to the differences in the mechanical behavior of the two implants. In another research paper, the authors studied cages with porous structure instead of solid one, concluding that the risk of subsidence can be reduced by decreasing the mismatch between the elastic moduli of the implant and vertebral bodies.[20]

The main novelty of the present study is the addition of a porous part included within a skeletal device made of the same bulk material. The reason for such a design choice was to evaluate potential improvements in the mechanical performance of the implants.

In more detail, the aim of this research is to verify the improvement of subsidence performance resulting from the introduction of micro lattice structures, which ensure a smoother contact pressure at the vertebrae-cage interfaces without modifying the solid structure, which guarantees the mechanical stability of the implant.

2 | MATERIALS AND METHODS

2.1 | Description of the devices

The investigated devices were two lumbar cages made of Ti-6Al-4V ELI (Grade 23) alloy and produced via Electron Beam Melting (EBM)

process. The Arcam Q10 3D printer was used to manufacture the devices. The Ti6Al4V ELI titanium alloy contained reduced levels of oxygen, nitrogen, carbon, and iron and its particle size distribution was between 45 and 100 μm. The partially porous (PP) device included an external solid shell, a porous micro lattice core and an upper and a lower endplate both with micro lattice structure (Figure 1A).

The selected unit cell of all the micro lattice parts was the rhombic dodecahedron (RD). The unit cell size was 3 mm for the core and 2 mm for the endplates. Parent material and micro lattice structures were investigated in a previous study.[21] The skeletal (S) device had the same external shell of the first case, but it did not include any micro lattice structure (Figure 1B). The nominal dimensions of the implant were the same in both cases: $48 \times 21 \times 9$ mm^3, where the height was obtained as the mean value between the anterior height (11 mm) and the posterior one (7 mm), while the thickness of the external shell had a constant value of 2 mm. The average value of surface roughness (S_a) was 20.7 μm and was measured by a confocal microscope (Leica DCM 3D, Leica Microsystems, Germany), as shown in Figure 2. Statistical analyses were made on an area of 0.64×1.54 mm^2 belonging to the cage, by means of LeicaMap 6.2 software. Such a scan was obtained by an extended topography with an EPI 20X-L objective in LeicaScan DCM 3D software. The z-scan covered a height of 600 μm with a z-step of 10 μm.

The data extracted from the surface, according to ISO25178 are reported in Table 1:

where: S_q is the root mean square height of the surface, S_{sk} is the skewness of height distribution, S_{ku} is the kurtosis of height distribution, S_p is the maximum height of peaks, S_v is the maximum height of valleys, S_z is the maximum height of the surface and S_a is the arithmetical mean height of the surface. The implants with high surface roughness improve osseointegration.[22] Thus, no additional treatment was performed after the EBM process. The devices were designed to be inserted by Lateral Lumbar Interbody Fusion (LLIF) approach. Lateral hollows allow the device fixation to the vertebral bodies during the implantation.

2.2 | Experimental investigations

Static compression tests were performed according to ASTM F2267 standard to analyze the subsidence of the implants. The test standard specifies the materials and methods for the axial compressive testing of the intervertebral body fusion devices. The tests aim to characterize the behavior of a device during the subsidence into the intervertebral bodies.The compression tests were carried out on an Italsigma FPF 25 universal testing machine equipped with a HBM U10M 12.5 kN load cell, at a constant speed of 0.1 mm/s and by applying a preload of 0.45 kN. The experimental tests were performed on both PP and S devices, with the aim of verifying the different behavior of the implanted cage with and without micro lattice structure. For evaluating the subsidence behavior, the devices were positioned between two polyurethane grade 15-test blocks, having dimensions

FIGURE 1 Devices object of the study: (A) with porous micro lattice core; (B) without porous micro lattice core

(A)   (B)
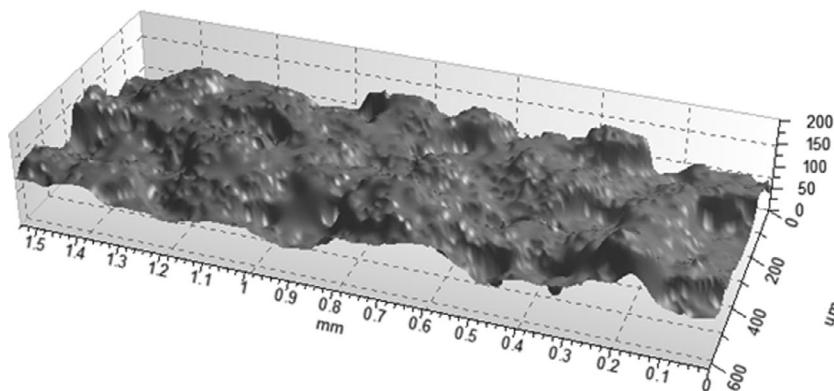
FIGURE 2 Surface analysis of the device

TABLE 1 Surface analysis results

Name	Value	Unit
S_q	25.91	μm
S_{sk}	0.22	
S_{ku}	3.72	
S_p	104.5	μm
S_v	103.7	μm
S_z	208.2	μm
S_a	20.72	μm

$60 \times 60 \times 40$ mm^3. The use of polyurethane foam was in conformity to ASTM F1839 standard, and it was intended to provide a consistent and uniform material having mechanical properties similar to human bone. The surface of the foam was machined with the same shape of the implant for a perfect matching at the interface between polyurethane and device, as shown in Figure 3.

As shown in Figure 4, the average height between the blocks including the cage was 4 mm. Therefore, this value was considered as the maximum crosshead displacement during the tests, which corresponded to the maximum subsidence.

The standard test procedure suggested a 10 mm intradiscal height H for lumbar implants at the center of the device, along the y-axis (Figure 4B). For the investigated cases, the footprints of the devices in the polyurethane blocks were deepened to make the assembly more stable and prevent sharing motion of the fixtures. Therefore, 4 mm height was the maximum value obtainable for the implants object of the study.

Visual inspection was carried out to evaluate the damage occurred during the compression tests and the deformation behavior of the polyurethane foam at the interface with both devices.

Moreover, CT analysis was performed with a Y.CT Vario (YXLON International GmbH, Hamburg, Germany) to validate the FE models by comparing the displacement of the polyurethane foam obtained from the experimental tests and FE analyses. CT scans were obtained with a focal spot size of 250 μm (smallest available), 190 kV voltage and 1.1 mA current and a 1 mm thick Cu filter between the tube and the specimen. The reconstruction was performed with a voxel resolution of $46.4 \times 46.4 \times 46.4$ μm^3 and a tomogram pixel resolution of 2048×2048. The dataset was processed by VGStudio Max 2.0 (Volume Graphics GmbH, Heidelberg, Germany) and the displacement was measured by the same software.

2.3 | Finite element models

The FE analyses were performed by using Altair HyperWorks® 14.0 (Altair Engineering, MI) package software. Hypermesh® software was used for mesh generation and boundary conditions definitions while Optistruct® software was used as implicit solver. The non-linear quasi-static FE model aimed to replicate the boundary conditions of the experimental tests but with the application of physiological loads. The first step involved FE structural analyses of both devices. Since the PP device included three different components, as described in Section 2.1, a tied contact was defined at the interfaces between the three different parts of the device to guarantee the actual structural continuity of the device produced via EBM. Tied contact produces rigid bond and prevents relative movements of the components. According to the mesh sensitivity test, in which element size of dimensions from 0.5 mm to 0.1 mm were analyzed, all the components were discretized using 0.2 mm first order tetrahedral elements. The following boundary conditions were applied: a compressive load of 1 kN, equal to twice the physiological one,[23] to verify the mechanical strength of the cage, and
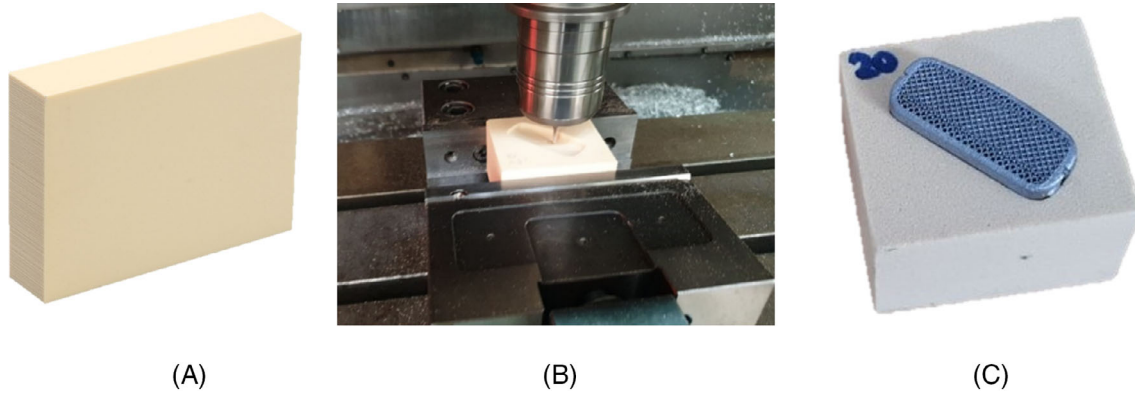
FIGURE 3 Tooling of Polyurethane foam blocks: (A) raw blocks; (B) CNC machining; (C) final result with a perfect fit of the device into the block
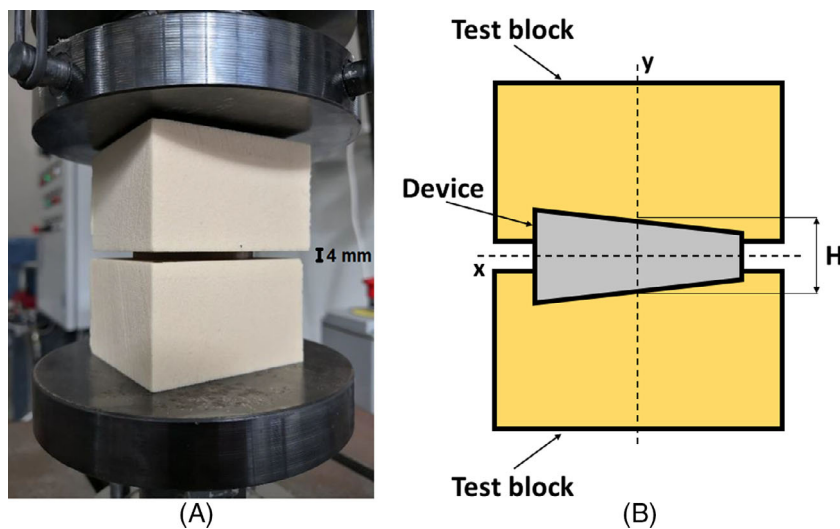

FIGURE 4 Polyurethane foam blocks with the cage implanted: (A) compression tests, (B) intradiscal height

fixed constraints in all directions. The material properties of the device were obtained from a previous study, in which experimental tests on both porous and bulk materials were carried out.[21] The micro lattice structure was modeled as an equivalent isotropic material having the mechanical properties of the porous Ti-6Al-4V ELI. The stress distribution and values were similar to the ones obtained with the RD unit cell. This assumption was considered acceptable by the authors because the stress distribution in the unit cells does not influence the subsidence phenomenon, which depends only by the contact at the interface between device and vertebra.

In the second step, the FE analyses of the polyurethane foam blocks with the implanted devices were validated. Two different models were developed, one with the PP cage and the other with the S cage. For both cases, the same method was applied to model the blocks, with the same geometry of that used in the compression tests. A mesh convergence analysis was performed and mesh transition was considered as the optimal choice: first order tetrahedral elements with higher density (0.4 mm size) were generated in the contact region between the foam and the device, while coarser mesh (4 mm element size) was used in the further zone (Figure 5). The contact interface between the device and the polyurethane foam was modeled by applying a static Coulomb friction coefficient equal to 0.4.[24–26] The polyurethane foam was

modeled as an isotropic material[27]; a summary of the material properties applied for the devices and the foam is reported in Table 2.

The boundary conditions were applied to reproduce the experimental test conditions, as shown in Figure 5, where magenta part is a fixed constraint in all directions, while red arrows represent a compressive load of 4 kN.

The FE analyses of both devices were validated by comparing the displacement obtained from FE simulations and from compression tests at a load of 4 kN, as well as by measuring, in the CT scans, the footprint left by the device into the PU blocks.

Finally, the condition referred to a person in stance position was simulated by applying a compressive physiological load of 0.5 kN.[23]

3 | RESULTS

3.1 | Compression tests

The compression tests were performed on both PP and S devices (with two repetitions for each type) to analyze the implant subsidence. The load–displacement curves obtained from the compression tests are reported in Figure 6.
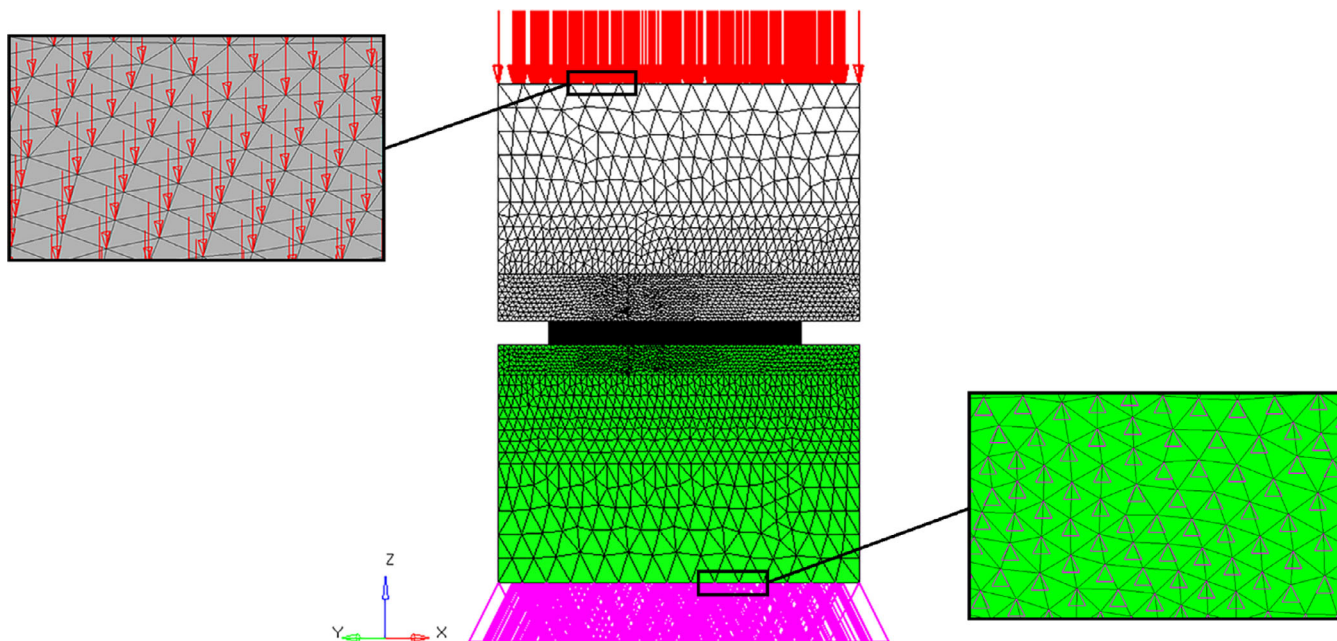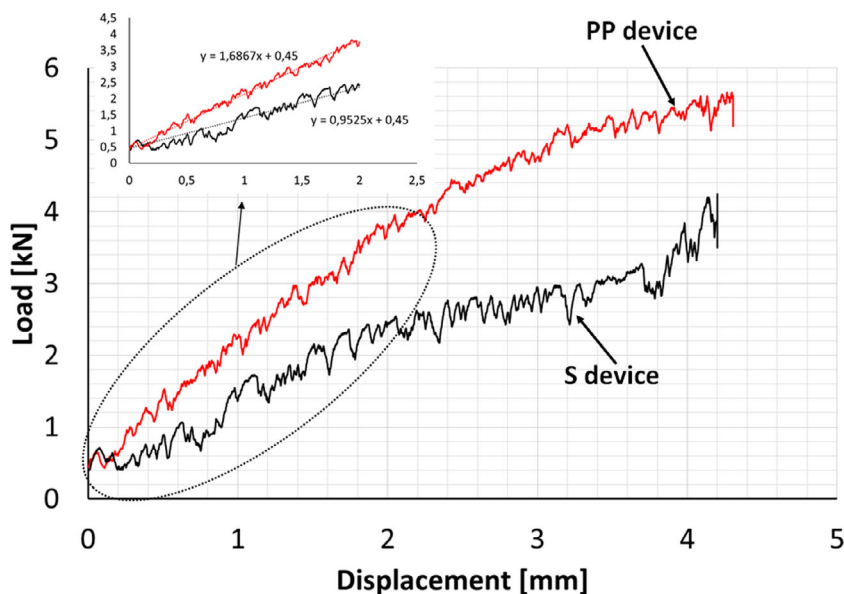
FIGURE 5 Boundary conditions of the FE subsidence analysis

TABLE 2 FE model material properties

	Ti6Al4V ELI Bulk	Ti6Al4V ELI RD_2 mm	Ti6Al4V ELI RD_3 mm	Polyurethane Foam
Young's modulus (GPa)	115	1.088	0.156	0.123
Poisson's ratio	0.33	0.33	0.33	0.3
Density (kg/m^3)	4430	1020	550	240.3

FIGURE 6 Load–displacement curves for PP device and S device

The ASTM F2267 standard test method establishes guidelines to measure test blocks deformation and to evaluate the subsidence of the intervertebral devices. It does not describe a method to evaluate their mechanical properties. Hence, in the standard test, the loads were small if compared to the mechanical strength of the device. The tests were stopped when the functional failure of the polyurethane foam occurred.

Since the tests on the PP device showed a good repeatability, the load–displacement curve reported in Figure 6 is the average one. The noise that characterized the curve for PP device was likely the result

of foam pores local collapse. The load trend for both devices was similar, but for the PP case, the absolute load values were higher. The maximum load achieved by the PP device was equal to 5.6 kN, corresponding to a displacement of 4.3 mm, while S device had a maximum load of 4 kN at a displacement of 4.2 mm. Thus, the micro lattice structure improved the subsidence behavior of the cage, by increasing the load achieved at a certain subsidence value. The FE models were validated by performing non-linear plastic analyses. The maximum load of 4 kN for the S device was considered as the reference value. This value was also used for the validation of the PP device model, yielding a displacement of 2.25 mm. The stiffness of the device-polyurethane foam system, and the energy absorbed during test, were calculated from the load–displacement curve. The stiffness was obtained from linear regression of the elastic curve (Figure 6): the PP device has significantly higher stiffness compared to the S device (Table 3). Higher stiffness values reduce the risk of subsidence, according to the current literature.[28] The absorbed elastic energy, calculated for the elastic part of the curve, and the total energy absorbed up to the maximum subsidence load were also obtained: PP device showed higher values than S device; the energy ratio was similar for the elastic energy and the total energy (Table 3).

3.2 | Visual inspection

The visual testing highlighted that the device including micro lattice guaranteed a better stress distribution at the interface between cage and blocks, as shown in Figure 7.

The presence of the micro lattice structure in the PP device produced a smooth stress distribution over the entire contact surface. Higher stress values were observed in the front zone of the contact surface, where higher displacement occurred. Nevertheless, these values did not result in higher load than the admissible one. For the S device, the contact at the interface was provided by the shell of the

TABLE 3 Device-foam stiffness and energy absorbed during experimental tests

	Stiffness (N/mm)	Total energy (J)	Elastic energy (J)
PP device	1686,7	15,46	4,28
S device	952,5	9,07	2,72
Ratio	1,77	1,7	1,58

implant. A more marked print was present all over the edge of the contact surface and in the central zone, due to overload. In the central zone, the overload could lead at the implant failure because the cortical bone is less thick than in the outer part of the vertebra; thus, it is able to sustain lower loads in this part.

3.3 | Finite element analyses

The structural analyses of the devices were carried out and the principal stresses for both devices subjected to a compressive load of 1 kN were evaluated. The results were compared to those obtained from a previous study for a device with similar geometry, that is designed using the same theoretical approach.[29] The stress values were smaller than the yield strength of the Ti-6Al-4 V ELI alloy, both in the solid structure[30] and in the porous structure.[21,31] Thus, no overload nor plastic behavior of the material were detected.

The displacement values were compared to those obtained in the experimental tests under a compressive load of 4 kN for validating the FE models of the polyurethane foam blocks with the implanted devices. The highest displacement values were detected in the front contact area. This behavior was confirmed by both the compression tests and the FE structural analyses. From CT inspection, it was observed that the deformed shape obtained from FE analyses was in good agreement with that obtained during the experimental tests as shown in Figure 8.

The footprints in the polyurethane foam blocks were compared, and the depth measured from CT scan was equal to 6.43 mm. In FE analysis, it was 6.29 mm, resulting in an error percentage of 2.18%, which can be considered acceptable. From the analysis of the contact pressure at the interface between polyurethane and devices, it was useful to observe the distribution of contact pressure, as shown in Figure 9.

The contact pressure was higher than the mechanical strength of the vertebral bone found in literature (red parts in Figure 9),[32] due to high value of the applied compressive load. The stress pattern was in accordance with the one observed in the experimental tests.

As expected from the experimental tests, the micro lattice structure guaranteed a smoother pressure distribution at the interface between cage and polyurethane. This behavior can be also observed in the curves of Figure 10, which refers to the sections marked in Figure 11.

The PP device (curves A and B) yielded some pressure peaks caused by singularity of the elements, that appeared in different parts of the
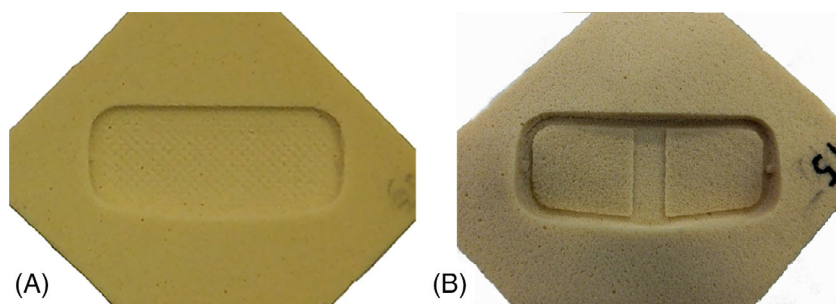

(A)   (B)

FIGURE 7 Stress distribution at the interface between polyurethane foam blocks and: (A) PP device, (B) S device

FIGURE 8 Comparison of the displacement in the front zone of the contact surface obtained with: (A) CT scan, (B) FE analysis
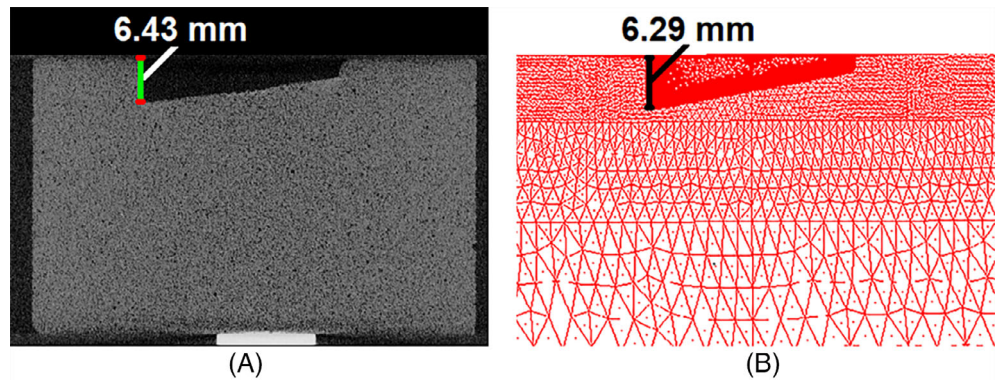

(A)

(B)

FIGURE 9 Contact pressure under a compressive load of 4 kN of the polyurethane foam blocks in the analyses with: (A) PP device, (B) S device
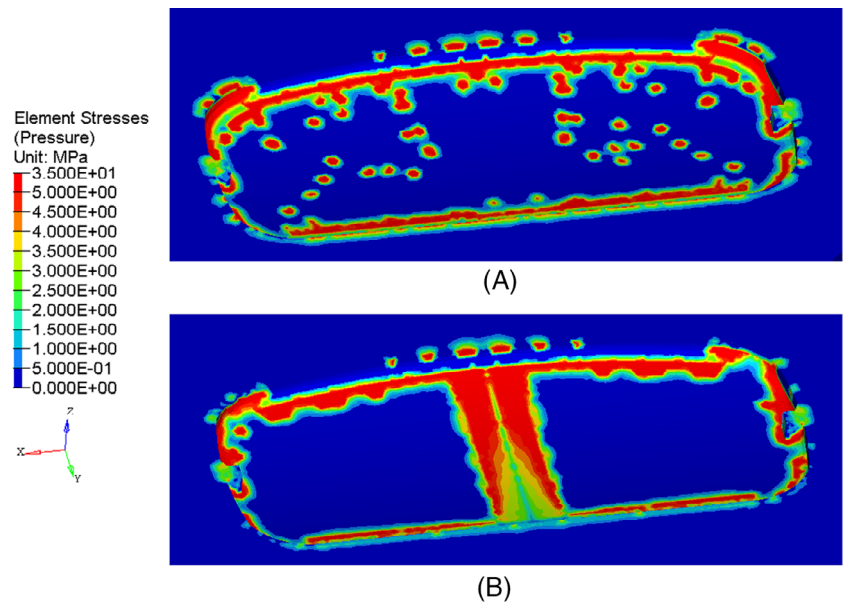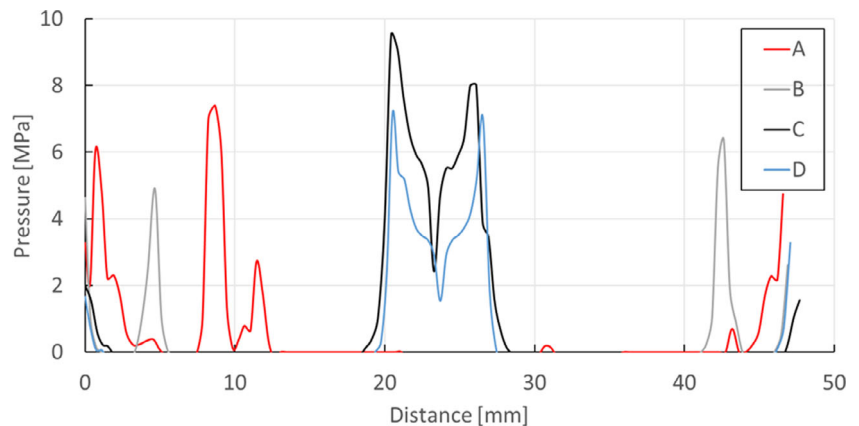

(A)

(B)

FIGURE 10 Pressure-distance curves at the interface between device and polyurethane blocks

contact interface for each section. The S device (curves C and D) presented for each section, pressure peaks in the central part of the contact interface, in the range between 20 and 30 mm. This trend led to overloading of the bone, which constantly bears high pressure values.

Finally, under a physiological compressive load of 0.5 kN, the distribution of contact pressure was the same of the previous cases, with lower values, as shown in Figure 12.

For the PP device, the contact pressure was smaller than the mechanical strength of the vertebral bone. For the S device, the values in the central zone were still smaller than the mechanical strength of the bone. Nevertheless, these values were very close to the bone compressive strength because the central part of the bone has lower mechanical properties than the external one.
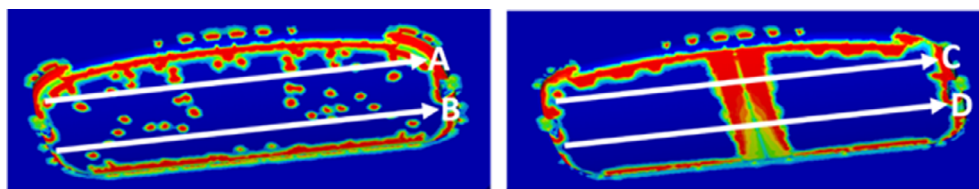
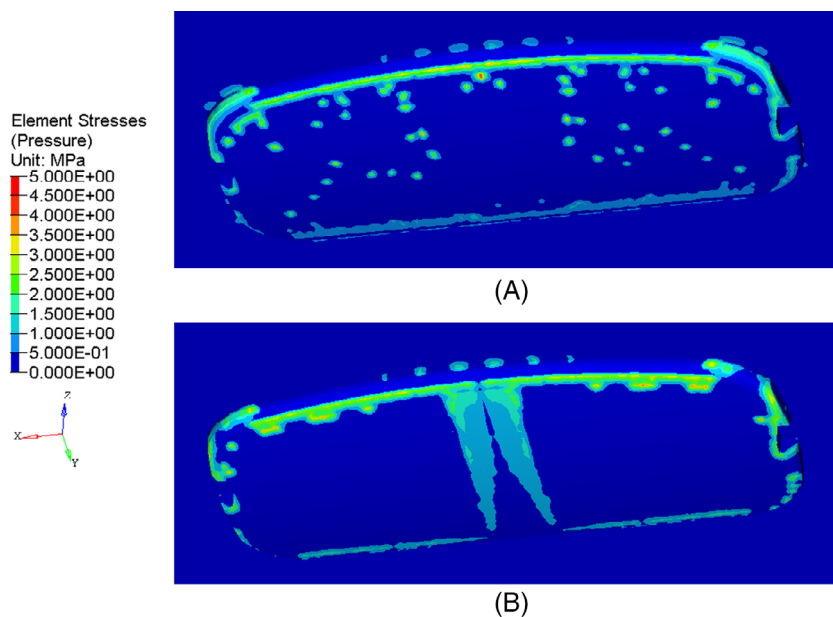FIGURE 11   Sections considered for the pressure-distance curves

FIGURE 12   Contact pressure under a compressive load of 0.5 kN of the polyurethane foam blocks in the analyses with: (A) PP device, (B) S device

4 | CONCLUSIONS

The subsidence phenomenon of lumbar intervertebral body fusion devices under the application of compressive load was investigated by means of experimental tests and finite element analyses. The contact pressure at the interface between implants and polyurethane foam blocks was evaluated by comparing a partially porous device and a skeletal device.

The experimental tests have shown that the subsidence risk is higher in the traditional device, which is characterized by lower stiffness, lower maximum load, and a smaller contact surface compared to the partially porous device. On the contrary, it was observed that the presence of micro lattice structure guaranteed a smoother pressure distribution at the contact interface, despite not having any structural function as confirmed in the FE analyses.

The porous structures are commonly used in the design of intervertebral body devices for multiple reasons.

The results of the present research do not aim at demonstrating that PP device has enhanced mechanical properties, since the peak stress values are comparable for the two analyzed devices. On the other hand, the results showed that the presence of micro lattice structure resulted in an optimal pressure distribution on the bone surface, decreasing the risk of subsidence. This behavior is particularly important in the lumbar region, in which vertebral bodies bear high compressive loads.

Both experimental and numerical results may be used in the design of novel intervertebral body fusion devices, considering the good agreement between the numerical results and the experimental data. In addition, they can be used to optimize the presence of both porous and bulk structure, to obtain more efficient devices.

The main advantage of the method used in the study is the possibility to validate FE analyses for a precise and careful design of the device. Nevertheless, the standard procedure did not consider the possibility to test the device behavior when a subject-specific design procedure is required for a peculiar geometry of the vertebra to be implanted. Such a limitation can be overcome by FEA, even though it gives an approximated result of the subsidence behavior since it is calibrated on PU foam. Another drawback of the method stands also in the lack of consideration of the mechanical properties of the bone to be implanted. This aspect can be also overcome by developing a FEA based on the mechanical properties obtained by CT scans, through the evaluation of the bone apparent density.

DATA AVAILABILITY STATEMENT
The data that support the findings of this study are available from the corresponding author upon reasonable request.

ORCID

Fabio Distefano https://orcid.org/0000-0002-0255-5857
Gabriella Epasto https://orcid.org/0000-0003-1372-5871

REFERENCES

1. Zhang Z, Li H, Fogel GR, Xiang D, Liao Z, Liu W. Finite element model predicts the biomechanical performance of transforaminal lumbar interbody fusion with various porous additive manufactured cages. *Comput Biol Med.* 2018;95:167-174. doi:10.1016/j.compbiomed.2018.02.016

2. Punt IM, Visser VM, Van Rhijn LW, et al. Complications and reoperations of the SB Charité lumbar disc prosthesis: experience in 75 patients. *Eur Spine J.* 2008;17:36-43. doi:10.1007/s00586-007-0506-8

3. Rundell SA, Isaza JE, Kurtz SM. Biomechanical evaluation of a spherical lumbar interbody device at varying levels of subsidence. *SAS Journal.* 2011;5:16-25. doi:10.1016/j.esas.2010.12.001

4. Dvorak MF, Kwon BK, Fisher CG, Eiserloh III HL 3rd, Boyd M, Wing PC. Effectiveness of titanium mesh cylindrical cages in anterior column reconstruction after thoracic and lumbar vertebral body resection. *Spine (Phila Pa 1976).* 2003;28:902-908. doi:10.1097/00007632-200305010-00012

5. Stieber JR, Donald GD. Early failure of lumbar disc replacement: case report and review of the literature. *J Spinal Disord Tech.* 2006;19:55-60. doi:10.1097/01.bsd.0000163414.53732.a3

6. Ji C, Yu S, Yan N, et al. Risk factors for subsidence of titanium mesh cage following single-level anterior cervical corpectomy and fusion. *BMC Musculoskelet Disord.* 2020;21:32. doi:10.1186/s12891-019-3036-8

7. Hussein AI, Mason ZD, Morgan EF. Presence of intervertebral discs alters observed stiffness and failure mechanisms in the vertebra. *J Biomech.* 2013;46:1683-1688. doi:10.1016/j.jbiomech.2013.04.004

8. Joshi A, Massey CJ, Karduna A, Vresilovic E, Marcolongo M. The effect of nucleus implant parameters on the compressive mechanics of the lumbar intervertebral disc: a finite element study. *J Biomed Mater Res–B Appl Biomater.* 2009;90B:596-607. doi:10.1002/jbm.b.31322

9. Calvo-Echenique A, Cegoñino J, Chueca R, Pérez-del Palomar A. Stand-alone lumbar cage subsidence: a biomechanical sensitivity study of cage design and placement. *Comput Methods Programs Biomed.* 2018;162:211-219. doi:10.1016/j.cmpb.2018.05.022

10. Bocahut N, Audureau E, Poignard A, et al. Incidence and impact of implant subsidence after stand-alone lateral lumbar interbody fusion. *Orthop Traumatol: Surg Res.* 2018;104:405-410. doi:10.1016/j.otsr.2017.11.018

11. Adam C, Pearcy M, McCombe P. Stress analysis of interbody fusion - finite element modelling of intervertebral implant and vertebral body. *Clin Biomech.* 2003;18:265-272. doi:10.1016/S0268-0033(03)00022-6

12. Rastegar S, Arnoux PJ, Wang X, Aubin CÉ. Biomechanical analysis of segmental lumbar lordosis and risk of cage subsidence with different cage heights and alternative placements in transforaminal lumbar interbody fusion. *Comput Methods Biomech Biomed Engin.* 2020;23:456-466. doi:10.1080/10255842.2020.1737027

13. Mohammad-Shahi MH, Nikolaou VS, Giannitsios D, Ouellet J, Jarzem PF. The effect of angular mismatch between vertebral endplate and vertebral body replacement endplate on implant subsidence. *J Spinal Disord Tech.* 2013;26:268-273. doi:10.1097/BSD.0b013e3182425eab

14. Lee JH, Jeon DW, Lee SJ, Chang BS, Lee CK. Fusion rates and subsidence of morselized local bone grafted in titanium cages in posterior lumbar interbody fusion using quantitative three-dimensional computed tomography scans. *Spine (Phila Pa 1976).* 2010;35:1460-1465. doi:10.1097/BRS.0b013e3181c4baf5

15. Tan JS, Bailey CS, Dvorak MF, Fisher CG, Oxland TR. Interbody device shape and size are important to strengthen the vertebra-implant interface. *Spine (Phila Pa 1976).* 2005;30:638-644. doi:10.1097/01.brs.0000155419.24198.35

16. Hsu CC. Shape optimization for the subsidence resistance of an interbody device using simulation-based genetic algorithms and experimental validation. *J Orthop Res.* 2013;31:1158-1163. doi:10.1002/jor.22317

17. Goel VK, Panjabi MM, Patwardhan AG, Dooris AP, Serhan H, American Society for Testing and Materials. Test protocols for evaluation of spinal implants. *J Bone Jt Surg–A.* 2006;88:103-109. doi:10.2106/JBJS.E.01363

18. Yuan W, Kaliya-Perumal AK, Chou SM, Oh JYL. Does lumbar Interbody cage size influence subsidence? *Biomech Study Spine (Phila Pa 1976).* 2020;45:88-95. doi:10.1097/BRS.0000000000003194

19. Chong ACM, Harrer SW, Heggeness MH, Wooley PH. Biomechanical evaluation of CIBOR spine interbody fusion device. *J Biomed Mater Res–B Appl Biomater.* 2017;105:1157-1168. doi:10.1002/jbm.b.33665

20. Lim KM, Park TH, Lee SJ, Park SJ. Design and biomechanical verification of additive manufactured composite spinal cage composed of porous titanium cover and PEEK body. *Appl Sci (Switzerland).* 2019;9:4258. doi:10.3390/app9204258

21. Epasto G, Palomba G, D'Andrea D, et al. Ti-6Al-4V ELI micro lattice structures manufactured by electron beam melting: effect of unit cell dimensions and morphology on mechanical behavior. *Mater Sci Eng A.* 2019;753:31-41. doi:10.1016/j.msea.2019.03.014

22. Rupp F, Scheideler L, Rehbein D, Axmann D, Geis-Gerstorfer J. Roughness induced dynamic changes of wettability of acid etched titanium implant modifications. *Biomaterials.* 2004;25:1429-1438. doi:10.1016/j.biomaterials.2003.08.015

23. Han K, Rohlmann A, Zander T, Taylor WR. Lumbar spinal loads vary with body height and weight. *Med Eng Phys.* 2013;35:969-977. doi:10.1016/j.medengphy.2012.09.009

24. Yu HY, Cai ZB, Zhou ZR, Zhu MH. Fretting behavior of cortical bone against titanium and its alloy. *Wear.* 2005;259:910-918. doi:10.1016/j.wear.2005.01.037

25. Kuiper JH, Huiskes R Friction and Stem Stiffness Affect Dynamic Interface Motion in Total Hip Replacement.

26. Viceconti M, Muccini R, Bernakiewicz M, et al (2000) Large-sliding contact elements accurately predict levels of bone implant micromotion relevant to osseointegration.

27. Suh PB, Puttlitz C, Lewis C, Bal BS, McGilvray K. The effect of cervical interbody cage morphology, material composition, and substrate density on cage subsidence. *J Am Acad Orthop Surg.* 2017;25:160-168. doi:10.5435/JAAOS-D-16-00390

28. Palepu V, Helgeson MD, Molyneaux-Francis M, Nagaraja S. The effects of bone microstructure on subsidence risk for ALIF, LLIF, PLIF, and TLIF spine cages. *J Biomech Eng.* 2019;141:031002. doi:10.1115/1.4042181

29. Epasto G, Distefano F, Mineo R, Guglielmino E. Subject-specific finite element analysis of a lumbar cage produced by electron beam melting. *Med Biol Eng Comput.* 2019;57:2771-2781. doi:10.1007/s11517-019-02078-8

30. Niinomi M. Mechanical properties of biomedical titanium alloys. *Mater Sci Eng A.* 1998;243:231-236. doi:10.1016/S0921-5093(97)00806-X

31. Li SJ, Xu QS, Wang Z, et al. Influence of cell shape on mechanical properties of Ti-6Al-4V meshes fabricated by electron beam melting method. *Acta Biomater.* 2014;10:4537-4547. doi:10.1016/j.actbio.2014.06.010

32. Adams MA, McNally DS, Chinn H, Dolan P. Posture and the compressive strength of the lumbar spine. *Clin Biomech.* 1994;9:5-14. doi:10.1016/0268-0033(94)90052-3